HHS Public Access

Author manuscript

Dev Neurosci. Author manuscript; available in PMC 2018 March 25.

Published in final edited form as:

Dev Neurosci. 2017 ; 39(1-4): 107–123. doi:10.1159/000456658.

Focal brain injury associated with a model of severe hypoxic-ischemic encephalopathy in nonhuman primates

Ryan M McAdams[1], **Ronald J McPherson**[1], **Raj P Kapur**[2], and **Sandra E Juul**[1]

[1]Department of Pediatrics, Division of Neonatology, University of Washington, Seattle, WA

[2]Department of Pathology, Seattle Children's Hospital, Seattle, WA

Abstract

Worldwide, hypoxic-ischemic encephalopathy (HIE) is a major cause of neonatal mortality and morbidity. To better understand the mechanisms contributing to brain injury and to improve outcomes in neonates with HIE, better preclinical animal models that mimic the clinical situation following birth asphyxia in term newborns are needed. In an effort to achieve this goal, we modified our nonhuman primate model of HIE induced by *in utero* umbilical cord occlusion (UCO) to include postnatal hypoxic episodes to simulate apneic events in human neonates with HIE. We describe a cohort of 4 near-term fetal *Macaca nemestrina* who underwent 18 min of *in utero* UCO, followed by Cesarean section delivery, resuscitation, and subsequent postnatal mechanical ventilation with exposure to intermittent daily hypoxia (3 min 8% O_2, 3–8 times daily x 3d). After delivery, all animals demonstrated severe metabolic acidosis (pH 7±0.12; mean, SD) and low Apgar scores (<5 at 10 min of age). Three of 4 animals had both electrographic (based on aEEG) and clinical seizures. Serial blood samples were collected and plasma metabolites were determined by two-dimensional gas chromatography coupled with time-of-flight mass spectrometry (GC × GC–TOFMS). The 4 UCO animals and a single non-asphyxiated animal delivered by Cesarean section, but without exposure to UCO or prolonged sedation, underwent magnetic resonance brain imaging on day of age 8. Thalamic injury was present on MRI in 3 UCO animals, but not the control animal. Following necropsy on day of age 8, brain histopathology revealed neuronal injury/loss and gliosis in portions of the ventrolateral thalamus in all 4 UCO, with 2 animals also demonstrating putamen/globus pallidus involvement. In addition, all 4 UCO animals demonstrated brainstem gliosis, with neuronal loss present in the midbrain, pons and lateral medulla in 3 of 4 animals. Transmission electron microscopy imaging of brain tissues was performed, which demonstrated ultrastructural white matter abnormalities, characterized by perinuclear vacuolation and axonal dilation, in 3 of 4 animals. Immunolabeling of Nogo-A, a negative regulator of neuronal growth, was not increased in injured brains compared to 2 control animals. Using GC × GC–TOFMS we identified metabolites previously recognized as potential biomarkers of perinatal asphyxia. The basal ganglia-thalamus-brain stem injury produced by UCO is consistent with the deep nuclear-brain stem injury pattern seen in human neonates after severe, abrupt hypoxic-ischemic insults. The UCO model permits timely detection of biomarkers

Corresponding Author: Sandra E. Juul, MD, PhD, University of Washington, Department of Pediatrics, Division of Neonatology, 1959 NE Pacific Street, HSB RR542D, UW Box 356320, Seattle, WA 98195-6320, Phone: 206-221-6814; Fax: 206-543-8926, sjuul@uw.edu.

associated with specific patterns of neonatal brain injury and it may ultimately be useful to validate therapeutic strategies to treat neonatal HIE.

Keywords

perinatal asphyxia; hypoxic-ischemic encephalopathy; magnetic resonance imaging; dexmedetomidine

Introduction

Intrapartum hypoxic events ("birth asphyxia") are a major cause of neonatal mortality responsible for approximately one in five of all neonatal deaths worldwide [1]. These intrapartum hypoxic events often result in hypoxic-ischemic encephalopathy (HIE), characterized by decreased consciousness, tone and reflexes, with clinical symptoms that include seizures, impaired respiration, poor feeding abilities, and apneic episodes [2,3]. Many questions persist regarding the underlying cellular, molecular and genetic mechanisms that may influence both the susceptibility of fetuses to develop HIE and their responses to treatment with therapeutic hypothermia. To address these questions and promote direct translation of experimental findings to the clinical setting, we developed a nonhuman primate model of perinatal asphyxia using *in utero* umbilical cord occlusion (UCO) to produce moderate to severe HIE [4].

The nonhuman primate model of UCO-induced perinatal asphyxia has evolved over time with the goal of closely modeling the brain injury patterns and clinical manifestations of human neonates with moderate to severe HIE. Initially, UCO was increased from 12 to 15 min to produce a degree of perinatal asphyxia that modeled the newborn population targeted for neuroprotection in the therapeutic hypothermia clinical trials [5,6]. UCO for 15 minutes was associated with encephalopathy by physical exam and aEEG findings, abnormal EEG, progressive spasticity, cognitive delay, transient kidney and liver biochemical dysfunction, feeding delay, and neuronal degeneration with gliosis on immunohistochemistry [4]. In 4 animals with UCO for 15 min, neurodevelopmental testing to 4 months of age (approx. 16 human months) demonstrated severe motor impairment in 2 vehicle control animals compared to only mild motor impairment in 2 animals treated with erythropoietin (Epo, 5,000 U/kg/dose at t = 0 and then 24 hours later). However, MRI evidence of structural brain injury in the first at 48–72 h of age or at 2 months of age was not detected in this model. In an effort to better replicate the morbidity of human neonates with moderate to severe HIE, the UCO was increased from 15 to 18 min (UCO_{18min}) and neurodevelopmental follow-up was extended to 9 months of age (approx. 36 human months) [7]. All asphyxiated primates met standard diagnostic criteria for human perinatal asphyxia (i.e., abnormal physical exam, acidosis, elevated lactate, large base deficits, and low Apgar scores). Brain volume comparison at 9 months versus at 1–3 days of age demonstrated decreased cerebellar (but not total brain, cortical, or basal ganglia) with UCO_{18min} compared to controls. Using diffusion tensor imaging, improved fractional anisotropy, relative anisotropy and volume ratios were apparent with early scans (24 and 72 h of age) in animals exposed to $UCO_{18\ min}$ treated with therapeutic hypothermia plus erythropoietin compared to $UCO_{18\ min}$ saline

animals. However, despite extending UCO to 18 min, neither the watershed nor basal ganglia findings characteristic of human HIE brain injury were detected in this model at either 1–3 days or 6–9 months of age.

The UCO model has enabled us to associate HIE with poor developmental outcomes [7], directly test the effects of combined neurotherapeutic treatments on developmental brain injury [8], and to characterize the circulating metabolome to identify potential biomarkers of HIE [9,10]. In an effort to produce a MRI-detectable structural brain injury pattern consistent with patterns seen in human neonates we further modified our model. When we attempted to induce structural brain injury by extending UCO beyond 18 minutes to 20 minutes (unpublished data), the animal mortality rate became unacceptable. Therefore, we considered postnatal factors present in newborns with HIE that might contribute to brain injury. Human newborns exposed to perinatal events resulting in HIE are often subjected to additional stressors postnatally that might aggravate their condition, such as bradycardia, intermittent apnea, and mechanical ventilation. We present evidence showing that animals subjected to *in utero* UCO followed by prolonged ventilation and intermittent apnea exhibit patterns of injury in the basal ganglia, thalamus, and brain stem that are precisely comparable to post-mortem injury effects observed in human neonates with severe HIE [11].

Methods and Animals

The Animal Care and Use Committees at the University of Washington in accordance with U.S. NIH guidelines approved all experimental procedures. An overview of the experimental UCO model used to produce HIE in *Macaca nemestrina* is summarized in figure 1.

Delivery and Resuscitation

Four *Macaca nemestrina* (pigtailed macaques) were delivered by hysterotomy under maternal general anesthesia (sevoflurane) 9 ± 2 days prior to term (173 days). One week of nonhuman primate life approximates one month of human life, so these animals are comparable to late preterm infants at birth. After incising the uterus, the umbilical cord was exteriorized while keeping amniotic fluid and the fetus inside. To simulate perinatal asphyxia, the umbilical cord was clamped for 18 minutes and a 2.5 French umbilical arterial catheter was inserted to permit all infusions and blood sampling. After delivery, animals were weighed and stabilized by a team of neonatologists using standardized neonatal resuscitation principles. Resuscitation included using endotracheal intubation, positive-pressure ventilation, chest compressions, and bolus epinephrine as needed. A heating pad, radiant warmer, and polyethylene sheet provided thermal support. Apgar scores were assessed at 1, 5, 10 and 20 minutes. Subdermal scalp electrodes were installed to record amplitude-integrated electroencephalography (aEEG) for 24 h. Animals were then moved into a customized thermal-neutral incubator and pulse oximetry and rectal temperature were monitored. A Dräger Babylog 8000 ventilator (Dräger, Lu beck, Germany) with humidifier, a Brainz BRM3 Monitor (Natus Medical Incorporated, Pleasanton, CA), infusion pumps, medical air/oxygen tanks and a battery with 120V AC inverter were mounted directly on the incubator to enable temporary portable operation.

Animal Care

Two infusion pumps provided parenteral nutrition (PN) and sedation. PN mixtures contained dextrose and 2% amino acids and electrolytes. Dextrose concentration (6 to 12%), electrolytes and infusion rate were adjusted individually based on monitoring. Animals were initially bolused with either morphine (100 μg/kg) or dexmedetomidine (DEX; 2 μg/kg) at 1 h and again at 6 h of age. Sedative infusions (1 mL/hr) began at 6 h of age and were formulated in 6% dextrose 2% protein solution to deliver 20 μg/kg/hr morphine or 0.3 μg/kg/hr DEX based on birth weight. Animals remained continuously sedated and received PN until necropsy on day 8. Sedation scoring was performed every 6 h beginning at 6 h of age using an escalating 1 to 4 ordinal scale to assess sleep, response to touch, arousal, and tone. Animals exhibiting clinical seizure activity were administered doses of phenobarbital 5 mg/kg until seizure activity stopped.

Postnatal intermittent hypoxia exposure

To simulate apnea with the intent to exacerbate the severity of HIE, animals were exposed to up to 8 daily episodes of hypoxia for the first 3 days of age as tolerated. Intubated animals were hand-ventilated with 8% O_2 for 3 min followed by 100% O_2 as needed for recovery. Heart rate and oxygen saturation (SpO_2) using a Nellcor (Pleasanton, CA) N-595 pulse oximeter were monitored and recorded during hypoxia exposure and recovery. The duration and frequency of hypoxia episodes was reduced individually for sensitive animals exhibiting poor tolerance (e.g. severe bradycardia or hypoxia with slow return to baseline).

Laboratory Analyses

Clinical arterial blood gases were monitored as clinically indicated, using a portable blood gas processor (iSTAT, Abaxis, Union City, CA). Blood samples (0.4 mL) for sedative pharmacokinetics (PK) and metabolomic measures were collected at 0, 0.25, 0.5, 1, 3, 6, 6.25, 48, 72, and 120 hours after the first sedative dose. Blood samples were collected in EDTA-coated tubes and spun at 1000G for 10 min and the plasma was aliquoted and frozen at −80ºC. Plasma concentrations of morphine and DEX were determined by ELISA.

MRI and Spectroscopy

At 8 days of age, animals underwent MRI and MRS brain imaging followed by necropsy as previously described.[7] A single non-asphyxiated *M. nemestrina* primate was delivered by Cesarean section, but without exposure to UCO or prolonged sedation, also underwent MRI/MRS at 8 days of age. This non-asphyxiated animal was included for comparative control MRI/MRS data only, since the animal did not undergo necropsy at day of age 8. MRI sequences included magnetization-prepared rapid gradient echo (MP-RAGE) high-resolution T_1-weighted imaging and single-voxel proton spectroscopy (MRS) acquired on a Phillips Achieva 3.0-tesla magnet with an X-series Quasar Dual gradient system. Custom fit 8- channel array head coils were used. For structural analysis, a 3-dimensional, high-resolution, T_1- weighted MP-RAGE protocol was used. For biochemical analysis, single-voxel MRS was acquired using a point-resolved spectroscopy pulse sequence centered on a 10 × 10 × 10 mm voxel on the right thalamus. The MP-RAGE sequence was reconstructed in real time to guide MRS voxel placement. Acquisition parameters included: TR = 2,000

ms; TE at 6 different echo times (32, 45, 65, 80, 100 and 150 ms); 2,048 complex free induction decay points, and 2,000 Hz spectral width. Absolute concentrations of short-echo (at TE = 32 ms) metabolites: *N*-acetyl aspartate (NAA), creatine (Cr), choline (Cho), myoinositol (Ins), glutamate (Glu) and glutamate + glutamine (Glx) were calculated using LCModel [12]. Absolute concentrations are reported in units that approximate millimolar concentrations. Partial volume corrections were made using the FSL segmentation software called FAST (Oxford, UK).

A historical cohort of 25 animals delivered by Cesarean section at 169±2 weeks' gestation, 12 control animals (4 male, 8 female) and 13 animals (6 male, 7 female) who underwent UCO for 15 (n=5) to 18 (n=8) min ($UCO_{15\text{-}18min}$), was included in this study for MRS comparison purposes. These 25 animals had MRS performed between 24 to 72 hrs of age using the abovementioned protocol. The $UCO_{15\text{-}18min}$ animals received saline treatment at 30 min, 24 h, 48 h, and 7 days of age as part of a study assessing the safety and effectiveness of erythropoietin plus therapeutic hypothermia in animals with HIE [8].

Transmission Electron Microscopy (TEM)

After perfusion, brains were removed and biopsy punches from the corpus callosum were collected and processed for TEM using 0.1M sodium cacodylate solution containing 4% paraformaldehyde/2% glutaraldehyde, cacodylate solution with 1% osmium tetroxide, serial ethanol dehydration, propylene oxide/EmBed 812 medium, then embedded and baked. Semi-thick sections were cut and toluidine blue stained before ultrathin sections (70 nM) were prepared on grids, stained with lead citrate, then multiple TEM images were captured at high (30,000×) and low (5,000×) magnifications (JEOL 1230, Peabody, MA). Captured TEM images from the 4 animals were reviewed in a blinded manner by a veterinary pathologist and compared to HE slides, and TEM images were assessed semi-quantitatively for the severity of white matter injury based on the presence of perinuclear vacuolation and/or axonal swelling. Artifact was present on the TEM images from animal 4, which confounded critical analysis.

Histology and Immunohistochemistry of Brain Tissue

Perfusion-fixed brain tissues were embedded in paraffin and four micron-thick sections from brainstem, thalamus and basal ganglia were stained with either hematoxylin and eosin (H&E) or immunostained using the Ventana Bench Mark Ultra automated immunostainer (Ventana Medical Systems, Tucson, AZ). Single target peroxidase-based labeling using anti-GFAP (1:400, DakoCytomation, Denmark) or anti-CD163 (1:200, Vector Laboratories, Burlingame, CA) primary antibodies was performed.

Brainstem tissues were embedded in paraffin and four micron-thick sections from the pons and medulla were H&E stained or immunostained using the Ventana Bench Mark Ultra automated immunostainer (Ventana Medical Systems, Tucson, AZ) according to the manufacturer's instructions. Sections were subjected to an antigen retrieval process of 8 minutes using Ventana's Cell Conditioner 1 (Ventana Medical Systems, Tucson, AZ) followed by GFAP detection using an anti-GFAP antibody (Ventana Medical Systems, predilute Ready to Use).

Staining for Nogo-A, a negative regulator of neuronal growth that has been shown to limit neural plasticity and recovery from brain injury [13], was performed to determine if this signaling protein was present in brain injury related to UCO plus postnatal hypoxia exposure. Dual immunofluorescence to localize GFAP and Nogo-A was performed on representative paraffin sections from the brains of each experimental animal and two controls. For controls, brain tissue was obtained from two *Macaca nemestrina* fetuses who were delivered by Cesarean section (one at 142 and one at 145 days gestation), immediately euthanized by barbiturate overdose followed by exsanguination and fetal necropsy with tissue fixation in 10% neutral buffered formalin. Coronal sections of the cerebral hemisphere at the level of the rostral lenticular nucleus (globus pallidus and putamen) were preincubated in 0.1M Citrate buffer (20 min in rice steamer), blocked with 5% goat serum/0.3% Triton X/ phosphate buffered saline for 2 hr, incubated overnight in rabbit anti-Nogo-A (1:1000; Abcam, Cambridge, MA) and mouse anti-GFAP (1:400; Dako Cytomation, Denmark), washed and incubated in secondary antibodies (1:500; anti-rabbit-Cy3, Jackson ImmunoResearch, West Grove, PA and anti-mouse-Dylight 488, Vector Laboratories, Burlingame, CA) and counterstained with DAPI. Digital images of the labeling were captured using Elements software (Nikon Corp. Tokyo, JP) with uniform capture settings used for all sections.

Plasma Metabolomics

Plasma metabolites were extracted, derivatized and detected using 2D gas chromatography coupled with time-of-flight mass spectrometry (GC × GC–TOFMS), as previously described [10]. Metabolites were identified using Chroma time of flight (TOF) software (LECO Corp., St. Joseph, MI) and analyzed with a parallel factor analysis (PARAFAC) algorithm to determine the m/z peak signal intensity normalized to total ion current. The signal ratio method was used to select the top 15 candidates for statistical comparisons.

Statistics

For parametric data, one-way ANOVA followed by post hoc tests (SPSS, Chicago, IL) or unpaired t-tests were performed as indicated in the text. ANOVA data are presented as means with standard error (SEM) for which *post-hoc* tests included *t*-test or Dunnett's test for multiple comparisons. In addition, Spearman rank-order correlation coefficients were calculated to compare nonparametric ordinal data as described. All comparisons were two-tailed with alpha ≤ 0.05.

Results

All 4 animals delivered after UCO_{18min} were flaccid, unresponsive to stimulation, and had no spontaneous respirations. All animals received positive-pressure ventilation and chest compressions during resuscitation, and animal 2 received epinephrine for low heart rate unresponsive to ventilation. Table 1 describes the birth indices including the weight, sex, and the number of days preterm, as well as initial blood gas values and Apgar scores that were indicative of perinatal asphyxia.

The aEEG tracings (not shown) from all animals showed burst suppression for 4 to 5 hours with subsequent elevation of baseline to normal around 6 hours of age after UCO. Three of the 4 animals exhibited electrographic and clinical seizures with onset ranging from 9 to 26 hours. Seizures were treated with phenobarbital and lasted 1–2 days in two animals (animals 2 and 3), but persisted for 7 days in one animal (animal 1).

Oxygen saturation (SpO_2) response to 3 min of hypoxia exposure were lower (unpaired t-test MS *vs.* DEX at 3 min) in the morphine-treated animals (animals 1 and 2) than the DEX-treated animals (animals 3 and 4) as seen in Figure 2. Neither heart rate response nor sedation scores appeared significantly different in relation to sedative treatment. At 3 min post hypoxia exposure, the mean SpO_2 was 23 ± 12% in morphine-treated vs 63 ± 5% in the DEX-treated animals. The SpO_2 returned to >98% within 1 min of recovery in all animals. In contrast to the consistent pattern of desaturation, the HR responses did not vary uniformly during hypoxia. In addition, tolerance to the postnatal hypoxia varied between animals so the number of episodes was adjusted individually (animal 1=23, animal 2=6, animal 3=13, and animal 4=21 total episodes over 3 days).

A single bolus of sedative (morphine or DEX) was given after resuscitation, and with a second bolus followed by sedative infusions initiated at 6 h of age and maintained until necropsy on day 9. Figure 3 presents the corresponding pharmacokinetic data showing plasma concentrations of morphine and DEX at scheduled time points. A battery of four sedation scores (sleep, arousal, touch response, tone) were recorded every 6 h for 7 days, but there were no differences for any of the scores (data not shown). There were no differences in adverse events based on sedation.

MRI and Spectroscopy

The MRI and MRS data were evaluated by a board-certified neurologist and compared to data from a contemporary non-study primate. Figure 4 contains T2 and FLAIR MRI images from each UCO animal collected just prior to necropsy on day of age 8. MRI imaging detected bilateral ventral posterolateral thalamus injury, which was evident in 3 of 4 UCO animals by with both T2-weighted and T2 fluid-attenuated inversion recovery (FLAIR) imaging (Fig 4). The control animal had normal MRI findings (images not shown). Diffusion-weighted images were normal for all animals (not shown).

MRS data of the 4 UCO_{18min} plus the single non-asphyxiated control animal are presented in Table 2. Historical comparison data was used to investigate potential MRS metabolite differences related to UCO_{18min} with and without postnatal hypoxia exposure. We previously reported MRS data obtained at 24–72 hr of age from 25 animals delivered by Cesarean section, including 12 control animals and 13 animals who underwent $UCO_{15\text{-}18min}$ without postnatal hypoxia exposure [8]. Similar to the current study animals, this historical group also had MRS acquired with a voxel on the right thalamus. In the 4 animals exposed to UCO_{18min} plus postnatal hypoxia the NAA/Cr ratio (mean ± SEM; 0.65±0.03) was lower compared to the historical UCO (0.73±0.02) and the historical control (0.79±0.02) animals (p=0.008) (ANOVA then post hoc testing of study *vs.* control).

Histology and Immunohistochemistry of Brain Tissue

Coronal sections from cerebral hemispheres of the UCO animals showed a similar pattern of histopathological changes with variable severity, and correlated well with MRI images. Foci of neuronal degeneration and hypercellularity due to reactive gliosis were present, particularly in the lateral thalamus, rostral caudate nucleus, and lenticular nucleus (globus pallidus and putamen) (Figure 5A). Other regions, including hippocampus, cortical gray and white matter, and most of the large white matter tracts showed little or no gliosis and no obvious neuronal loss. However, mild increased gliosis in the corpus callosum was apparent in the more severely injured animals (animals 3 and 4). Cerebellar tissue was only available for animals 1, 2, and 4. No cerebellar abnormalities were detected in animals 1 and 2, but animal 4 demonstrated Purkinje cell drop out and Bergmann gliosis. Immunostaining confirmed accumulation of activated microglia (CD163+) and astrocytosis (GFAP+) in sites of injury, including the lateral thalamus corresponding to the region of hyperintensity detected by MRI (Figure 5B). These lesions were fairly discrete and bordered by minimally gliotic tissue, even in the most severely affected brains.

Grossly, the brainstems were normal but, in all 4 animals gliosis was present. Three cases (animals 2, 3, and 4) exhibited severe bilateral symmetric neuronal loss and gliosis in dorsolateral tegmentum, paragigantocellularis lateralis, dorsal reticular nuclei, and gliosis in the nucleus tractus solitarius, dorsal motor nucleus X and inferior olive, but no pathology of the hypoglossal nucleus, white matter tracts or vasculature. Figure 6 presents stained images from animal 3 and shows that subarachnoid hemorrhage was also present in this case. In contrast, animal 1 showed less severe pathology with diffuse gliosis, but no obvious apparent neuronal loss. A summary of the brain histopathological findings is presented in Table 3.

Dual immunofluorescence labeling was conducted to assess the GFAP and Nogo-A expression because expression of the latter has been observed in other models of brain injury. Nogo-A, while mainly expressed in oligodendrocytes, is also found in other neural cell types, such as astrocytes,[14] so co-labeling with GFAP, a marker of reactive astrocytes, was performed to exclude Nogo-A-expressing astrocytes. In the thalamus and corpus striatum of control fetal brains, minimal GFAP immunoreactivity was present (Figure 7D) and Nogo-A was detected in the cytoplasm of many oligodendroglial cells (Figure 7F). In contrast, gliotic foci in the thalamus and corpus striatum were highly enriched in GFAP+ astrocytes (Figure 7C), but showed no consistent increase in the density or fluorescent intensity of Nogo-A+ cells (Figure 7E). As expected, Nogo-A and GFAP did not co-localize, consistent with expression in oligodendroglia and astrocytes, respectively (Figure 7G).

Transmission Electron Microscopy

TEM images taken of the corpus callosum were evaluated and compared to H&E images from the same region. Ultrastructural white matter abnormalities, including perinuclear vacuolation and/or axonal dilation, were apparent in 3 of 4 animals. Figure 8 presents light microscopy and TEM images comparing animal 1, who had mild white matter injury, to animal 3, who had more severe white matter injury. Animal 2 had similar TEM findings as animal 3, and animal 4 appeared to have the most severe white matter injury, although artifact on TEM confounded critical assessment of this animal.

Plasma Metabolomics

Hundreds of metabolites were detected by GC × GC–TOFMS in plasma collected from the 4 animals. PARAFAC signal ratios were sorted to select the top 15 metabolites for *post hoc* analysis. Table 4 lists the average signal intensity values for the top 15 metabolites at baseline (0 h), immediately after resuscitation (0.1 h), and at one day of age (24 h). Table 4 is sorted to distinguish metabolites that peaked immediately after UCO (4A), gradually increased after birth (4B) or were not significantly affected (4C). Based on TEM and histology images, ordinal scores of severity of white matter injury were assigned so that Spearman r correlations between metabolite concentrations and severity of injury could be performed at each time point. In baseline cord blood, choline and *myo*-inositol both correlated negatively with injury (both r -0.948, $P < 0.001$), at 5 min dextrose correlated negatively with injury (r -0.948, $P < 0.001$), and at 24 h erythropentonic acid correlated negatively with injury (r -0.950, $P < 0.001$).

Discussion

The primate UCO model of HIE was developed to provide translational information about the metabolic, neurologic, and behavioral consequences of birth asphyxia [7,8,10]. Consistent with those reports, UCO produced moderate-to-severe HIE manifested by abnormal physical findings and blood gas parameters that satisfied established entry criteria used to qualify human infants in trials studying therapeutic hypothermia [5,6]. However, despite incremental increases of the UCO duration from 12 to 18 min, this model lacked evidence of MRI-detectable brain injury consistent with patterns seen in human neonates with HIE. Efforts to achieve MRI-detectable brain injury by extending the UCO beyond 18 min resulted in excessive mortality. Therefore, our model was modified to include postnatal mechanical ventilation and hypoxia exposure to better simulate the clinical scenario seen in neonates with moderate- to-severe HIE. Animals were also delivered slightly earlier, since nonhuman primate brain maturation is accelerated compared to human development. We report on a cohort of animals that underwent UCO for 18 min, similar to animals described in previous experiments [8], with the current 4 UCO animals also exposed to postnatal mechanical ventilation, intermittent hypoxia to simulate apnea, and prolonged sedation. These added postnatal factors, which were not part of our previous model, likely contributed to brain injury involving the ventral posterolateral thalamus as demonstrated on MRI at 8 days of age in 3 of the 4 animals.

In the 1970’s, Myers et al. demonstrated that acute, profound asphyxia produced predominantly deep gray matter lesions involving the basal ganglia and thalamus, compared to prolonged partial asphyxia, which produced cerebral white matter injury [15]. Most newborns with basal ganglia and thalamic injury on MRI have a history of acute and profound asphyxia, consistent with a clinical history of uterine or umbilical cord rupture, placental abruption, traumatic delivery, umbilical cord kinking, Apgar score < 5 after 5 min, and umbilical cord pH < 7 [16]. Miller et al. described two pathological patterns of brain injury detected by MRI (performed at a median of 6 days of age; range, 1–24 days) in 173 term newborns with HIE: watershed predominant and basal ganglia/thalamus predominant [17]. Compared to normal and watershed predominant patterns, the basal ganglia/thalamus

predominant pattern was associated with increased emergent Cesarean section delivery, intensive resuscitation after delivery, the most severe clinical encephalopathy and seizures, the lowest Mental Development Index of the Bayley Scales of Infant Development II, and the most severe neuromotor impairments at 30 months of age follow-up. Similar to the human neonates with basal ganglia/thalamus injury described by Miller et al., the 4 animals described in our cohort analysis required intensive resuscitation after delivery, had evidence of clinical encephalopathy and demonstrated seizure activity (3 of 4 animals).

This pilot study is the first to detect thalamic lesions on MRI in our nonhuman primate model of perinatal asphyxia. Postnatal hypoxia episodes, prolonged sedation, or the stress of prolonged ventilation (all factors that are common in critically ill human infants) may have contributed to the vulnerability of the ventral posterolateral thalamus in the setting of HIE. MRI data from 500 term HIE infants demonstrated that 75% of patients had some degree of thalamic injury [18]. In fact, when abnormal motor outcomes were correlated with patterns of MRI injury, thalamic injury was associated with the most severe motor abnormalities and was predictive of cerebral palsy (CP) [19]. Although hypoxic-ischemic injury has been the speculative cause of HIE-related thalamic damage, definitive conclusions have been elusive in part because timing of injury is often unknown, and MRI imaging and histological data have not been obtained within the same time frame [20]. The current study addresses this issue because the mechanism of injury is known (i.e., UCO) and both MRI and brain tissues for histological analysis were collected at 8 days of age. Three of 4 animals in the current study had MRI evidence of bilateral ventral posterolateral thalamic injury. The posterior and lateral ventral thalamic nuclei are the most vulnerable of thalamic nuclei to total asphyxia injury [15]. While sufficient concurrent controls were not available in the current study to compare MRS findings, comparison to animals from a previous study of UCO_{18min} [8] suggest that the addition of postnatal factors (e.g., hypoxia, mechanical ventilation, and prolonged sedation) affected MRS metabolite expression. The 4 animals exposed to UCO_{18min} plus postnatal hypoxia had a lower mean NAA/Cr ratio compared to the historical controls (Table 2). The decreased NAA/Cr ratio, a metabolic marker reflecting the functional status of neurons and axons in the brain, implies neuronal or axonal loss or dysfunction [21]. The decreased NAA/Cr ratio in the UCO_{18min} plus postnatal hypoxia animals compared to historical animals subjected to UCO_{18min} alone may suggest worse brain injury in the current model, however, MRS data were obtained at different time points between the current and historical animals so caution is warranted when interpreting these comparative data. Given the MRI, MRS, and brain pathology findings, the current experimental paradigm may be a suitable model of deep nuclear-brain stem injury pattern seen in human neonates with HIE associated with severe, abrupt hypoxic-ischemic insults.

Acquired brain injuries resulting from in utero hypoxic-ischemic events can be associated with damage to neuronal populations (e.g., basal ganglia and cortex) and cerebral white matter (e.g., cellular necrosis and axonal damage), which may lead to CP. For over a decade, there has been a call for better animal models to study the pathogenesis of white-matter injury associated with CP in term infants,[22] with recognition that a more thorough knowledge of oligodendrocyte development and physiology is essential for understanding the pathobiology of HIE [23]. We previously reported that UCO for 15 to 18 minutes resulted in death or moderate-to-severe CP in 43% of saline treated and 44% of TH treated

animals followed to 9 months of age in a term nonhuman primate model of perinatal asphyxia that included 56 *Macaca nemestrina* [8]. We speculated that our current UCO_{18min} model, which included postnatal hypoxic episodes, would also produce animals with CP if long-term follow-up was feasible. Therefore, we investigated whether Nogo-A expression, which is associated with disrupted myelin formation in oligodendrocytes, would be present in our model of severe HIE. Nogo-A, a member of the reticulon family mainly expressed in oligodendrocytes,[24] is a master regulator of CNS plasticity that can restrict structural remodeling and hinder axon regeneration during injury [13,14,25]. In adult animal models, inhibition of Nogo-A improves plastic adaptations and promotes functional recovery after CNS injury [26]. While animals exposed to UCO_{18min} and postnatal hypoxia demonstrated anti-Nogo-A staining of oligodendrocytes in the thalamic and striatal regions, anti-Nogo-A staining was also demonstrated in the two control animals. Due to limited animal numbers, our study cannot rule out a role for Nogo-A limiting functional recovery and neural repair following hypoxic ischemia-induced brain injury. Further studies in preterm and term animal models are needed to determine if Nogo-A is involved in the pathogenesis of HIE and the development of CP.

Critical care of newborns with moderate-to-severe HIE often requires sustained mechanical ventilation, which is frequently associated with prolonged sedation of patients [27]. In our model, prolonged sedation of mechanically-ventilated HIE animals was feasible using either morphine or DEX, an α2-adrenergic receptor agonist that is often used in neonatal intensive care units for sedation and pain management [28,29]. While sedation with DEX may be beneficial for neonates with HIE based on animal models [30–32], PK data in the setting of HIE are lacking. The sedation scores and PK data we collected suggest that morphine and DEX provide suitable sedation in HIE animals, however our small study numbers prevent any definitive conclusions regarding the safety and efficacy of these sedatives in the setting of HIE.

Animal models permit direct study of the pathophysiological mechanisms underlying disease states. Neonatal rodent models are advantageous because pups exhibit postnatal brain growth analogous to third trimester human development and litters are readily produced and simple to manage. Techniques used to create perinatal hypoxic brain injury in rodents involve unilateral ligation of the common carotid artery combined with hypoxia [33], prolonged hypoxia [34], or temporary occlusion of the middle cerebral artery [35]. The principal disadvantages of neonatal rodent models are related to their lissencephalic brain organization, lower white to gray matter ratio compared to primates and their more limited behavioral repertoire. Unlike rodents, nonhuman primate brain development and complexity are similar to those in humans, allowing for complex neurocognitive testing over time [36–39].

Despite many attractive attributes akin to human neonates, numerous problems are inherent in working with non-human pregnant primates as models of human neonatal HIE. Beyond the expense of the model, the existing ambiguities surrounding human neonatal HIE, such as the plethora of unanswered questions regarding the underlying etiologies that lead to moderate-to-severe HIE phenotype, make accurate animal model development a challenge. The non-human pregnant primate model requires exposure to general anesthesia to perform

isolation and clamping of the fetal umbilical cord, analogous to an ex utero intrapartum treatment procedure (EXIT procedure), in which the baby is partially delivered through the opening of a midline classical Cesarean section of the anesthetized mother's abdomen and uterus, but remains attached by its umbilical cord to the placenta. During this EXIT procedure, an umbilical artery catheter is placed, which can be difficult, but is necessary in order to obtain blood gases after delivery. In human neonates who develop HIE, poor fetal reactivity often leads to an emergency Cesarean, and therefore the sequence of anesthesia may be reversed to that of our model (i.e., anesthesia, then hypoxia-ischemia in nonhuman primates versus hypoxia-ischemia, then anesthesia in humans). The role of infection or abruption in human HIE is not addressed by our model, and while placental abnormalities may play a significant role in human HIE development, the placenta in the nonhuman primate UCO model is unlikely a factor in the pathologic process since the clamped umbilical cord is the intended cause of injury. Although the UCO model is imperfect, because of the many analogous features to human neonates with HIE, we are confident that preclinical testing of neuroprotective strategies that may translate to human infants will be best accomplished using a nonhuman primate model [8,40].

We previously examined changes in plasma metabolite concentrations in nonhuman primates associated with normal birth compared to animals exposed to perinatal asphyxia [9,10]. Several of the metabolites detected in this previous analysis were also identified in the current report, including *myo*-inositol and glutamate, and also arachidonic, fumaric, succinic, propanoic and erythropentonic acid. These plasma metabolites, which can be detected using GC × GC–TOFMS even with a limited number of available samples, appear to be biomarkers of perinatal asphyxia. Many of these markers are associated with general biochemical pathways and/or the tricarboxylic acid (TCA) cycle pathway. For example, *myo*-inositol is the precursor to inositol trisphosphate [41], which is a key mediator of signaling and regulatory functions such as gene expression [42], fat metabolism [43], and calcium homeostasis [44]. The amino acid glutamate is a signaling molecule and a key factor in cellular reduction-oxidation (redox) reactions [45]. Fumaric and succinic acid, TCA cycle intermediates necessary for aerobic redox metabolism, demonstrated a transient postnatal increase following UCO. At birth, the abrupt transition from a relatively hypoxic intrauterine to a normoxic extrauterine environment oxygen may produce oxidative stress [46] and, therefore, fetal mechanisms may be in place to upregulate signaling factors that mediate redox reactions [47]. The effects of perinatal asphyxia, an event associated with an extreme hypoxic to hyperoxic birth transition, on these oxidative stress pathway signaling factors needs further study, but may involve TCA cycle intermediates. In the current animals, and in the prior study, we observed that several TCA cycle intermediates were acutely elevated while other molecules (e.g. *myo-inositol*, glutamate et al) were gradually elevated. This expression pattern suggests that birth transition involves separate metabolic processes, both which are detectable in the plasma metabolome [9].

The UCO model of HIE is a sophisticated effort to develop a translational platform for identifying biomarkers that correlate with asphyxia-induced injury and for testing neurotherapeutic strategies to mitigate HIE. Our current pilot study, which describes a cohort of animals with UCO-induced HIE who underwent prolonged ventilation, sedation, and repeated hypoxia exposure, has many limitations. This study was limited by size, it lacked

proper control animals, did not include brain stereology, and did not include long-term outcomes. The small sample size hindered statistical analysis and prevented definitive conclusions regarding the observed changes in plasma biomarkers, structural sex-dependent long-term abnormalities after neonatal ischemia[48], and comparative effects of sedatives in the setting of HIE secondary to UCO_{18min}. In addition, our pathohistological investigation did not include staining for all cell types and regions relevant to HIE. In a recent study by Pagida et al, involving 15 human neonates (14 delivered at or near term, 1 preterm) mainly delivered by emergency cesarean section (11/15), subjects with neuropathological lesions consistent with abrupt/severe perinatal hypoxic/ischemic injury demonstrated intense immunohistochemical tyrosine hydroxylase expression in the majority of locus coeruleus neurons, a finding which the author's suggest may lead to monoaminergic neurotransmission dysregulation and predispose survivors to long-term psychiatric disorders with or without neurological problems [49]. Future UCO studies in nonhuman primates may benefit from a broader repertoire of immunohistochemical staining (e.g., tyrosine hydroxylase expression or neural stem and progenitor cells)[49,50] in order to better correlate abnormalities present in human neonates with HIE. Despite the small sample size, this pilot study was a necessary step for model refinement and provided useful information relevant to human newborns with HIE. The plasma metabolite profile corroborates previous findings from animals that have undergone perinatal asphyxia, and suggest that specific TCA cycle intermediates are altered in response to perinatal asphyxia exposure. This non-hypothesis driven analysis of plasma metabolites will foster future hypothesis driven studies that will improve our capacity to diagnose and treat neonatal conditions.

Our UCO_{18min} plus postnatal hypoxia model adds to Myers previously described model of basal ganglia/thalamus [15] injury since it provides contemporary approaches to assess brain injury and detect potential biomarkers, including MRI/MRS, and metabolomic data. This modification of our previous model, which adds several stressors to the 18 minutes of hypoxia ischemia, raises the question of whether postnatal factors may contribute to the poor outcomes of infants who present with moderate to severe encephalopathy. While extremely time intensive, this UCO_{18min} plus postnatal hypoxia/stress nonhuman primate model may be useful for understanding injury mechanisms, potential biomarkers, and therapeutic strategies in neonates with HIE.

Acknowledgments

Statement of Financial Support: This project was supported in part by NIH grants UL1 RR025014 and the ARRA supplement 3UL1 RR025015-0353 and P51 RR000166 from the National Center for Research Resource (NCRR), its contents are solely the responsibility of the authors and do not necessarily represent the official view of NCRR, NIH, or the Institute of Translational Health Sciences or the UW Primate Center. The authors have no financial associations, ties to products or conflicts of interest to disclose.

We would like to give thanks to Hannah Kinney and Robin Haynes for helpful direction and expertise, thanks to Jessica Snyder for reviewing the transmission electron microscopy images, Brittany Baker, Sarah Ramelli, Marianne Bricker, Kelly Ledbetter, Brian Phillips, Nina Natarajan and Todd Richards for expert assistance, and special thanks to the Washington National Primate Research Center personnel Cliff Astley, Audrey Baldessari, Bruce Brown, Noelle McKain, Clayton Ferrier and Tom Burbacher, and to Kristina Adams-Waldorf for providing brain tissues.

References

1. Liu L, Johnson HL, Cousens S, Perin J, Scott S, Lawn JE, Rudan I, Campbell H, Cibulskis R, Li M, Mathers C, Black RE. Child Health Epidemiology Reference Group of WHO Unicef. Global, regional, and national causes of child mortality: an updated systematic analysis for 2010 with time trends since 2000. Lancet. 2012; 379:2151–2161. [PubMed: 22579125]
2. American College of Obstetricians and Gynecologists. Executive summary. Neonatal encephalopathy and neurologic outcome. Obstetrics & Gynecology. 2014; 123:896–901. [PubMed: 24785633]
3. Takenouchi T, Kasdorf E, Engel M, Grunebaum A, Perlman JM. Changing pattern of perinatal brain injury in term infants in recent years. Pediatr Neurol. 2012; 46:106–110. [PubMed: 22264705]
4. Juul SE, Aylward E, Richards T, McPherson RJ, Kuratani J, Burbacher TM. Prenatal cord clamping in newborn Macaca nemestrina: a model of perinatal asphyxia. Dev Neurosci. 2007; 29:311–320. [PubMed: 17762199]
5. Shankaran S, Laptook AR, Ehrenkranz RA, Tyson JE, McDonald SA, Donovan EF, Fanaroff AA, Poole WK, Wright LL, Higgins RD, Finer NN, Carlo WA, Duara S, Oh W, Cotten CM, Stevenson DK, Stoll BJ, Lemons JA, Guillet R, Jobe AH. National Institute of Child H, Human Development Neonatal Research N. Whole-body hypothermia for neonates with hypoxic-ischemic encephalopathy. N Engl J Med. 2005; 353:1574–1584. [PubMed: 16221780]
6. Gluckman PD, Wyatt JS, Azzopardi D, Ballard R, Edwards AD, Ferriero DM, Polin RA, Robertson CM, Thoresen M, Whitelaw A, Gunn AJ. Selective head cooling with mild systemic hypothermia after neonatal encephalopathy: multicentre randomised trial. Lancet. 2005; 365:663–670. [PubMed: 15721471]
7. Jacobson Misbe EN, Richards TL, McPherson RJ, Burbacher TM, Juul SE. Perinatal asphyxia in a nonhuman primate model. Dev Neurosci. 2011; 33:210–221. [PubMed: 21659720]
8. Traudt CM, McPherson RJ, Bauer LA, Richards TL, Burbacher TM, McAdams RM, Juul SE. Concurrent erythropoietin and hypothermia treatment improve outcomes in a term nonhuman primate model of perinatal asphyxia. Dev Neurosci. 2013; 35:491–503. [PubMed: 24192275]
9. Beckstrom AC, Humston EM, Snyder LR, Synovec RE, Juul SE. Application of comprehensive two-dimensional gas chromatography with time-of-flight mass spectrometry method to identify potential biomarkers of perinatal asphyxia in a non-human primate model. Journal of chromatography A. 2011; 1218:1899–1906. [PubMed: 21353677]
10. Beckstrom AC, Tanya P, Humston EM, Snyder LR, Synovec RE, Juul SE. The perinatal transition of the circulating metabolome in a nonhuman primate. Pediatric research. 2012; 71:338–344. [PubMed: 22391633]
11. Volpe, J. Neurology of the Newborn. 5. Philadelphia, PA: W. B. Saunders Company; 2008.
12. Provencher SW. Estimation of metabolite concentrations from localized in vivo proton NMR spectra. Magn Reson Med. 1993; 30:672–679. [PubMed: 8139448]
13. Schwab ME, Strittmatter SM. Nogo limits neural plasticity and recovery from injury. Curr Opin Neurobiol. 2014; 27:53–60. [PubMed: 24632308]
14. Rolando C, Parolisi R, Boda E, Schwab ME, Rossi F, Buffo A. Distinct roles of Nogo-a and Nogo receptor 1 in the homeostatic regulation of adult neural stem cell function and neuroblast migration. The Journal of neuroscience : the official journal of the Society for Neuroscience. 2012; 32:17788–17799. [PubMed: 23223298]
15. Myers RE. Two patterns of perinatal brain damage and their conditions of occurrence. American journal of obstetrics and gynecology. 1972; 112:246–276. [PubMed: 4621486]
16. Sie LT, van der Knaap MS, Oosting J, de Vries LS, Lafeber HN, Valk J. MR patterns of hypoxic-ischemic brain damage after prenatal, perinatal or postnatal asphyxia. Neuropediatrics. 2000; 31:128–136. [PubMed: 10963099]
17. Miller SP, Ramaswamy V, Michelson D, Barkovich AJ, Holshouser B, Wycliffe N, Glidden DV, Deming D, Partridge JC, Wu YW, Ashwal S, Ferriero DM. Patterns of brain injury in term neonatal encephalopathy. The Journal of pediatrics. 2005; 146:453–460. [PubMed: 15812446]

18. Okereafor A, Allsop J, Counsell SJ, Fitzpatrick J, Azzopardi D, Rutherford MA, Cowan FM. Patterns of brain injury in neonates exposed to perinatal sentinel events. Pediatrics. 2008; 121:906–914. [PubMed: 18450893]
19. Ferrari F, Todeschini A, Guidotti I, Martinez-Biarge M, Roversi MF, Berardi A, Ranzi A, Cowan FM, Rutherford MA. General movements in full-term infants with perinatal asphyxia are related to Basal Ganglia and thalamic lesions. J Pediatr. 2011; 158:904–911. [PubMed: 21232764]
20. Haynes RL, Billiards SS, Borenstein NS, Volpe JJ, Kinney HC. Diffuse axonal injury in periventricular leukomalacia as determined by apoptotic marker fractin. Pediatric research. 2008; 63:656–661. [PubMed: 18520330]
21. Watanabe H, Fukatsu H, Katsuno M, Sugiura M, Hamada K, Okada Y, Hirayama M, Ishigaki T, Sobue G. Multiple regional 1H-MR spectroscopy in multiple system atrophy: NAA/Cr reduction in pontine base as a valuable diagnostic marker. J Neurol Neurosurg Psychiatry. 2004; 75:103–109. [PubMed: 14707317]
22. Johnston MV, Ferriero DM, Vannucci SJ, Hagberg H. Models of cerebral palsy: which ones are best? J Child Neurol. 2005; 20:984–987. [PubMed: 16417847]
23. Silbereis JC, Huang EJ, Back SA, Rowitch DH. Towards improved animal models of neonatal white matter injury associated with cerebral palsy. Dis Model Mech. 2010; 3:678–688. [PubMed: 21030421]
24. Schwab ME. Functions of Nogo proteins and their receptors in the nervous system. Nature reviews Neuroscience. 2010; 11:799–811. [PubMed: 21045861]
25. Kempf A, Schwab ME. Nogo-A represses anatomical and synaptic plasticity in the central nervous system. Physiology. 2013; 28:151–163. [PubMed: 23636261]
26. Zorner B, Schwab ME. Anti-Nogo on the go: from animal models to a clinical trial. Annals of the New York Academy of Sciences. 2010; 1198(Suppl 1):E22–34. [PubMed: 20590535]
27. Roka A, Melinda KT, Vasarhelyi B, Machay T, Azzopardi D, Szabo M. Elevated morphine concentrations in neonates treated with morphine and prolonged hypothermia for hypoxic ischemic encephalopathy. Pediatrics. 2008; 121:e844–849. [PubMed: 18381513]
28. Chrysostomou C, Schmitt CG. Dexmedetomidine: sedation, analgesia and beyond. Expert Opin Drug Metab Toxicol. 2008; 4:619–627. [PubMed: 18484919]
29. McAdams RM, McPherson RJ, Kapur R, Phillips B, Shen DD, Juul SE. Dexmedetomidine reduces cranial temperature in hypothermic neonatal rats. Pediatr Res. 2015; 77:772–778. [PubMed: 25751572]
30. Laudenbach V, Mantz J, Lagercrantz H, Desmonts JM, Evrard P, Gressens P. Effects of alpha(2)-adrenoceptor agonists on perinatal excitotoxic brain injury: comparison of clonidine and dexmedetomidine. Anesthesiology. 2002; 96:134–141. [PubMed: 11753013]
31. Paris A, Mantz J, Tonner PH, Hein L, Brede M, Gressens P. The effects of dexmedetomidine on perinatal excitotoxic brain injury are mediated by the alpha2A-adrenoceptor subtype. Anesth Analg. 2006; 102:456–461. [PubMed: 16428542]
32. Sato K, Kimura T, Nishikawa T, Tobe Y, Masaki Y. Neuroprotective effects of a combination of dexmedetomidine and hypothermia after incomplete cerebral ischemia in rats. Acta Anaesthesiol Scand. 2010; 54:377–382. [PubMed: 19860751]
33. Rice JE 3rd, Vannucci RC, Brierley JB. The influence of immaturity on hypoxic-ischemic brain damage in the rat. Annals of neurology. 1981; 9:131–141. [PubMed: 7235629]
34. Stewart WB, Ment LR, Schwartz M. Chronic postnatal hypoxia increases the numbers of cortical neurons. Brain research. 1997; 760:17–21. [PubMed: 9237513]
35. Ashwal S, Cole DJ, Osborne S, Osborne TN, Pearce WJ. A new model of neonatal stroke: reversible middle cerebral artery occlusion in the rat pup. Pediatric neurology. 1995; 12:191–196. [PubMed: 7619184]
36. Burbacher TM, Grant KS. Methods for studying nonhuman primates in neurobehavioral toxicology and teratology. Neurotoxicol Teratol. 2000; 22:475–486. [PubMed: 10974586]
37. Kochunov P, Castro C, Davis D, Dudley D, Brewer J, Zhang Y, Kroenke CD, Purdy D, Fox PT, Simerly C, Schatten G. Mapping primary gyrogenesis during fetal development in primate brains: high-resolution in utero structural MRI of fetal brain development in pregnant baboons. Front Neurosci. 2010; 4:20. [PubMed: 20631812]

38. Rilling JK. Comparative primate neuroimaging: insights into human brain evolution. Trends Cogn Sci. 2014; 18:46–55. [PubMed: 24501779]
39. Burbacher TM, Grant KS, Worlein J, Ha J, Curnow E, Juul S, Sackett GP. Four decades of leading-edge research in the reproductive and developmental sciences: the Infant Primate Research Laboratory at the University of Washington National Primate Research Center. Am J Primatol. 2013; 75:1063–1083. [PubMed: 23873400]
40. Sackett GP, Ruppenthal GC, Davis AE. Survival, growth, health, and reproduction following nursery rearing compared with mother rearing in pigtailed monkeys (Macaca nemestrina). American journal of primatology. 2002; 56:165–183. [PubMed: 11857653]
41. Downes CP, Macphee CH. myo-inositol metabolites as cellular signals. European journal of biochemistry /FEBS. 1990; 193:1–18.
42. Steger DJ, Haswell ES, Miller AL, Wente SR, O'Shea EK. Regulation of chromatin remodeling by inositol polyphosphates. Science. 2003; 299:114–116. [PubMed: 12434012]
43. Rapiejko PJ, Northup JK, Evans T, Brown JE, Malbon CC. G-proteins of fat-cells. Role in hormonal regulation of intracellular inositol 1,4,5-trisphosphate. The Biochemical journal. 1986; 240:35–40. [PubMed: 3103610]
44. Streb H, Irvine RF, Berridge MJ, Schulz I. Release of Ca2+ from a nonmitochondrial intracellular store in pancreatic acinar cells by inositol-1,4,5-trisphosphate. Nature. 1983; 306:67–69. [PubMed: 6605482]
45. McEntee WJ, Crook TH. Glutamate: its role in learning, memory, and the aging brain. Psychopharmacology. 1993; 111:391–401. [PubMed: 7870979]
46. Saugstad OD. Update on oxygen radical disease in neonatology. Current opinion in obstetrics & gynecology. 2001; 13:147–153. [PubMed: 11315869]
47. Maron JL, Johnson KL, Parkin C, Iyer L, Davis JM, Bianchi DW. Cord blood genomic analysis highlights the role of redox balance. Free radical biology & medicine. 2010; 49:992–996. [PubMed: 20566327]
48. Breu M, Zhang J, Porambo M, Pletnikov MV, Goeral K, Kakara M, Johnston MV, Fatemi A. Diffusion Tensor Imaging Abnormalities in the Cerebral White Matter Correlate with Sex-Dependent Neurobehavioral Deficits in Adult Mice with Neonatal Ischemia. Dev Neurosci. 2016; 38:83–95. [PubMed: 26977597]
49. Pagida MA, Konstantinidou AE, Korelidou A, Katsika D, Tsekoura E, Patsouris E, Panayotacopoulou MT. The Effect of Perinatal Hypoxic/Ischemic Injury on Tyrosine Hydroxylase Expression in the Locus Coeruleus of the Human Neonate. Dev Neurosci. 2016; 38:41–53. [PubMed: 26647061]
50. Kwak M, Lim S, Kang E, Furmanski O, Song H, Ryu YK, Mintz CD. Effects of Neonatal Hypoxic-Ischemic Injury and Hypothermic Neuroprotection on Neural Progenitor Cells in the Mouse Hippocampus. Dev Neurosci. 2015; 37:428–439. [PubMed: 26087836]

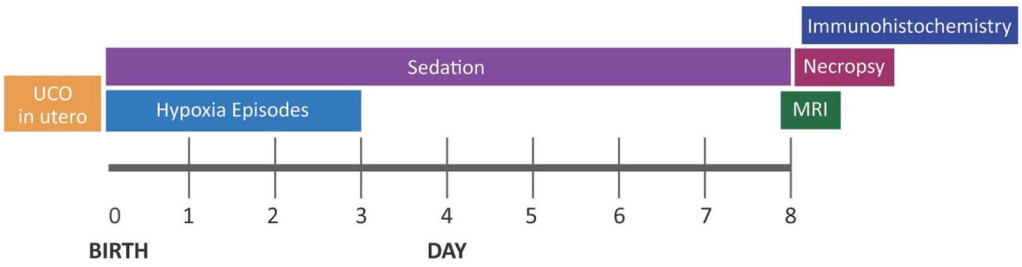

Figure 1.

An overview of the procedures and assessments for the nonhuman primate model of perinatal asphyxia. Animals received sedative infusions with either morphine (n=2) or dexmedetomidine (n=2) beginning at 6 h of age. Hypoxia episodes were induced during the first 3 days of age by exposing animals to 8% oxygen for 3 min to simulate apnea (range 6–21 episodes/animal). UCO = umbilical cord occlusion, MRI = Magnetic resonance imaging.

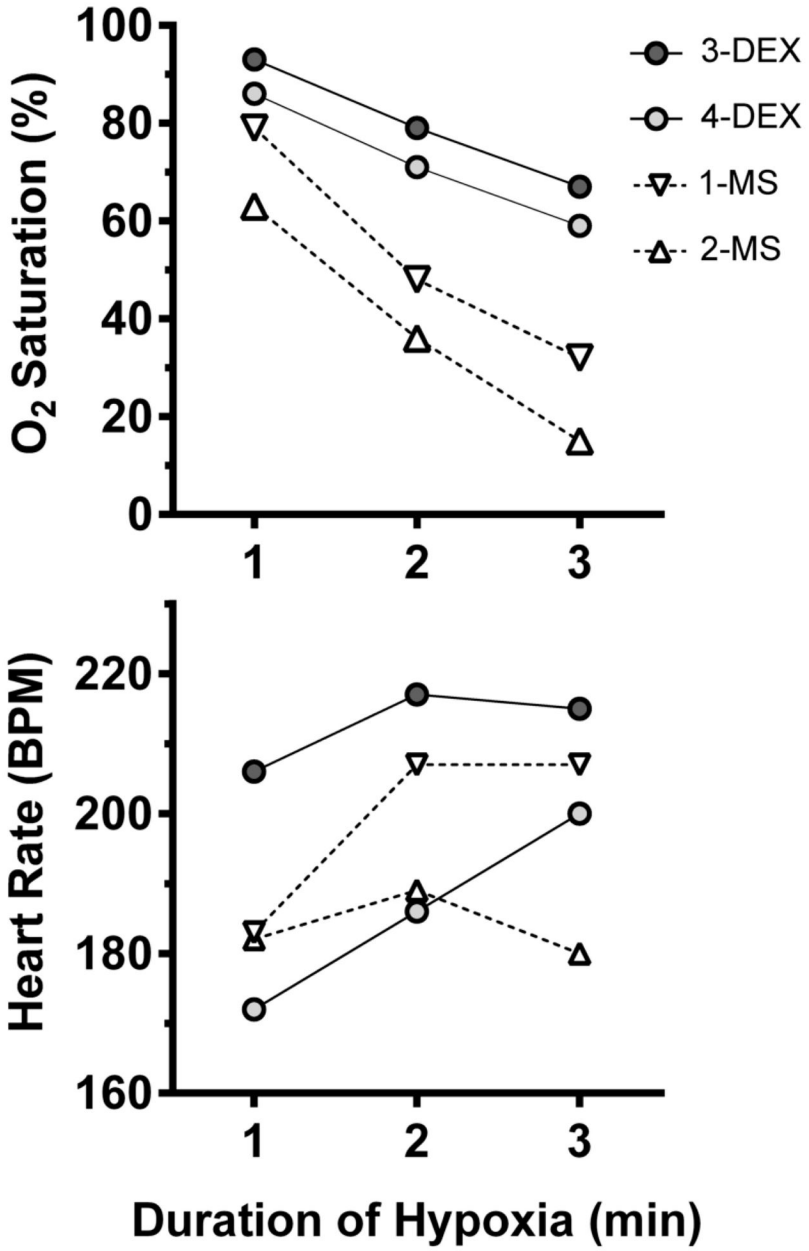

Figure 2.

Plots show the time course of changes in oxygen saturation (top panel) and heart rate (bottom panel) recorded from individual animals (1–4) during exposure to 8% hypoxia to simulate apnea for 3 min. Data points are the average of all measurements for each animal from repeated exposures (range 6–21 episodes/animal) performed during the first 3 days of age. Animals 1 and 2 received a continuous morphine (MS) at 20 μg/kg/h and animals 3 and 4 received a continuous dexmedetomidine (DEX) infusion at 0.3 μg/kg/h.

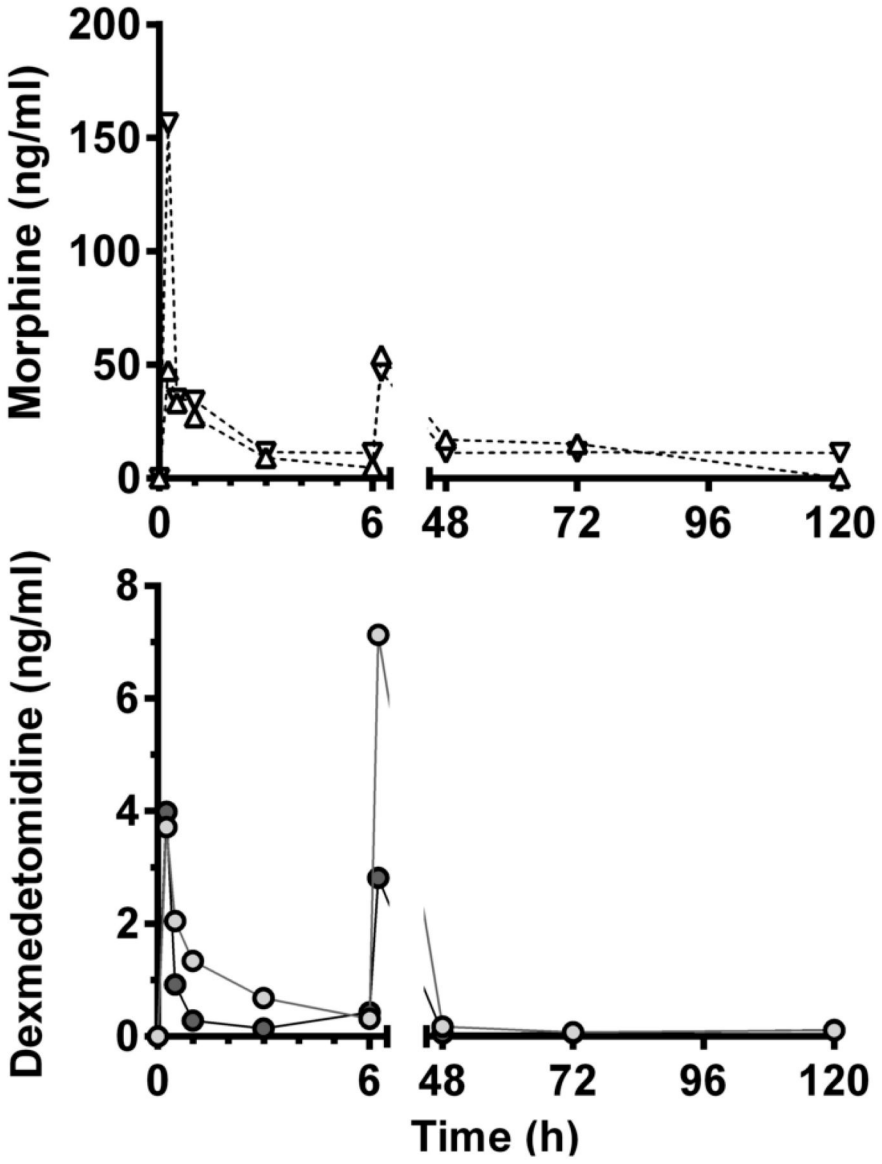

Figure 3.

Plots show the plasma concentrations of morphine (triangles, top panel) in animals 1 and 2 or dexmedetomidine (circles, bottom panel) in animals 3 and 4 measured from individual animals at scheduled intervals. Half-life ($t_{1/2}$) and rate constant (κ) were calculated using data for the first 6 hours, after which time a second bolus was administered and continuous infusions were initiated (one phase decay, morphine: $t_{1/2}$ = 7.5 min, κ = 5.5 ; DEX: $t_{1/2}$ = 9.6 min, κ = 4.2). Dosing for morphine was 100 μg/kg bolus (at 1h and 6h) then 20 μg/kg/h after 6h, and for DEX was 2 μg/kg bolus (at 1h and 6h) then 0.3 μg/kg/h infusion after 6h.

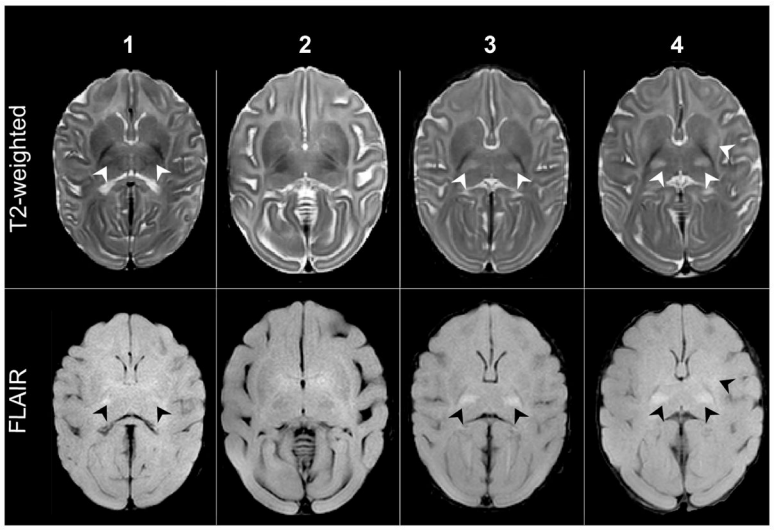

Figure 4.

MRI images recorded from four individual 8-day-old primates exposed to umbilical cord occlusion for 18 min plus postnatal mechanical ventilation and hypoxic episodes while under continuous sedation with either morphine or DEX. The numbers 1–4 on the top of each MRI image column indicate the animal number that corresponds to the T2-weighted and FLAIR images in each column. MRI T2-weighted and Fluid-attenuated inversion recovery (FLAIR) imaging revealed bilateral hyperintensity present in the posterior thalamus of 3 of the 4 animals (highlighted by arrows). In addition, animal 4 has evidence of unilateral hyperintensity in the putamen nucleus (the anterior arrow).

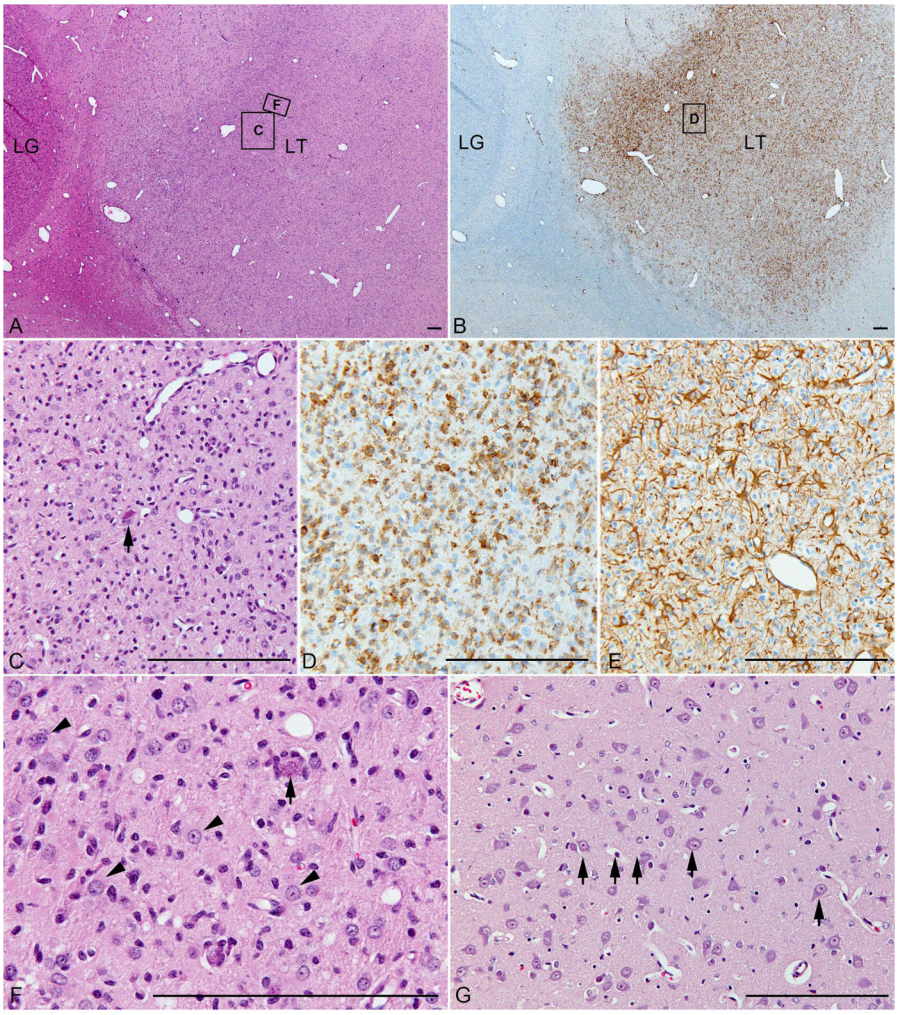

Figure 5.

Histological and immunostained images from an infarct in the lateral thalamus (LT) of animal 4. (A) A geographic zone of hypercellularity is evident in the lateral thalamus (boxes indicate regions of higher magnifications displayed in C and F), just medial to the lateral geniculate nucleus (LG, H&E-stain). In this focus, neurons are lost or degenerating (arrows in C and F) and reactive astrocytes (arrowheads) abound. Adjacent sections demonstrate that the hypercellularity is due in part to infiltration by (B, with box indicating region of higher magnification displayed in D) CD163-immunoreactive activated microglia and (E) GFAP-immunopositive reactive astrocytes. (G) A histological field in the adjacent medial portion of the thalamus shows intact neurons (arrows) and a normal density of relatively inconspicuous non-reactive astrocytes and microglia. Scale bars are 200 μm.

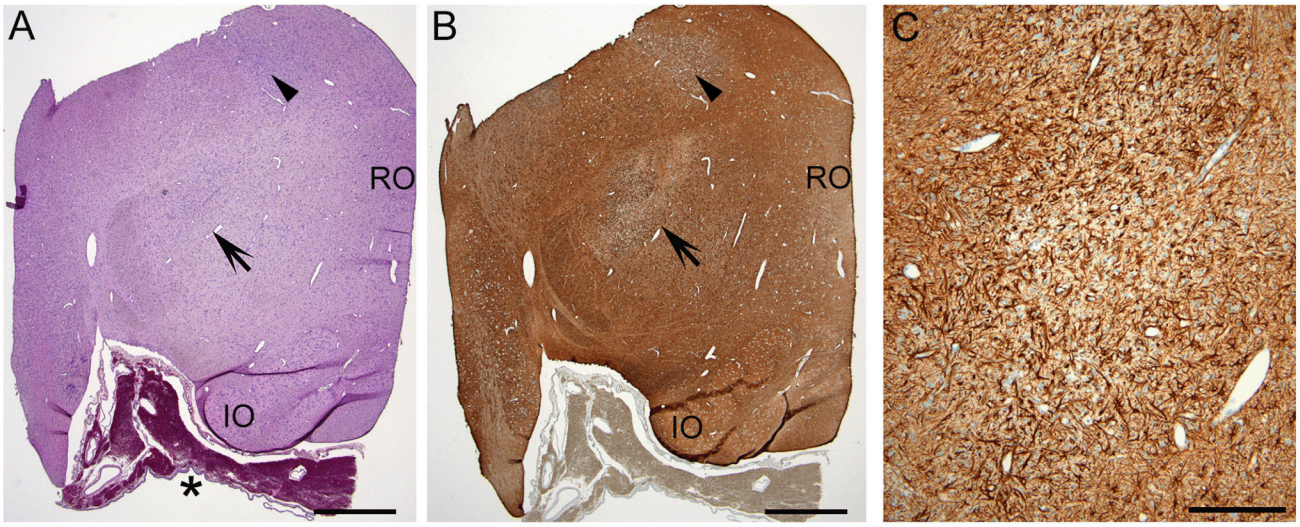

Figure 6.

Shown are hemisected sections of medulla taken from animal 3 and labeled for the raphe obscurus (RO) and the inferior olive (IO). A low power H&E stain (A) and GFAP immunostain (B) reveals the area of the focal scarring in the nucleus tractus solitarius (NTS, arrowhead) and the reticular formation (arrow). An asterisk (*) denotes the ventral subarachnoid hemorrhage. Panel C contains a higher magnification image depicting GFAP-immunopositive reactive astrocytes in the reticular formation derived from the region of the arrow tip in panel B. Scale bar length for panels A and B is 1mm, and panel C is 200 μm.

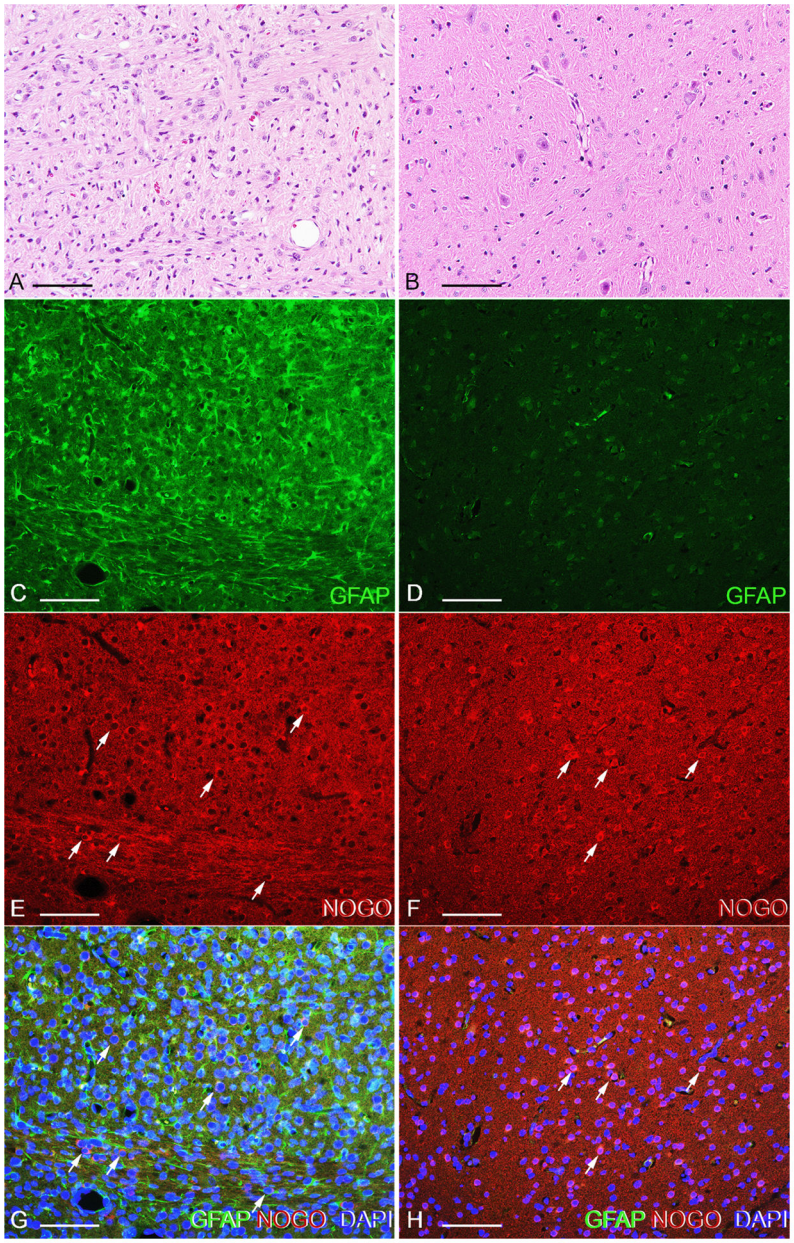

Figure 7.

H&E (A,B) and dual immunofluorescence (C-H) images from the putamen of animal 4 (A,C,E,G) versus a control fetus (B,D,G,H). Marked hypercellularity is present in the putamen of the experimental animal due in part to accumulation of GFAP+ astrocytes (C). Nogo-A immunofluorescence highlights the perikarya of oligodendroglial cells (E,F), which are GFAP-negative and showed no consistent difference in density or intensity of immunoreactivity between experimental and control animals. Scale bars = 100 μm.

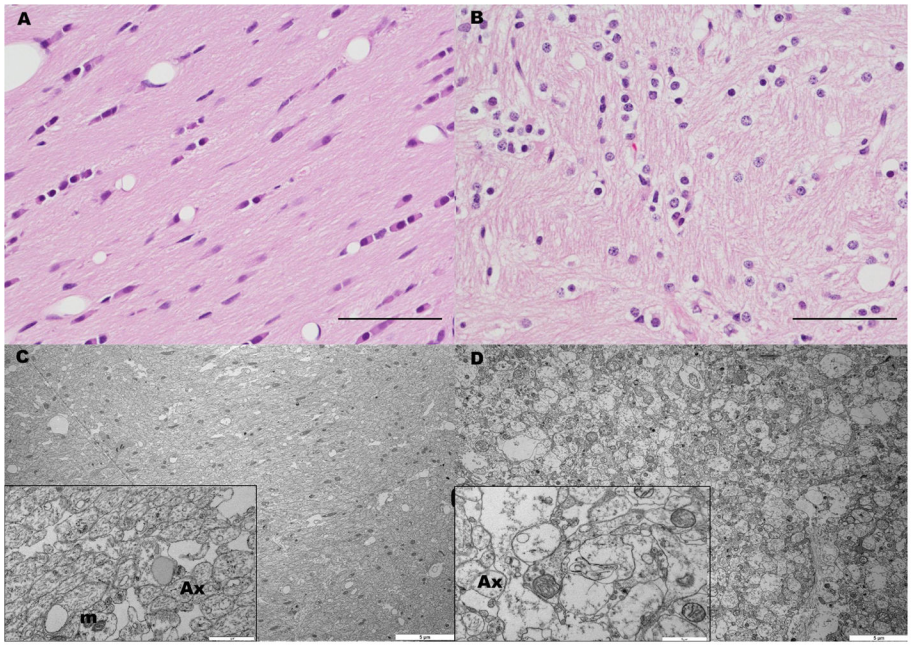

Figure 8.

Light microscopic and ultrastructural images of white matter (cerebral white matter and corpus callosum) from asphyxiated non-human primates. Panels A (animal 1) and B (animal 3) present H&E-stained images (bar = 50 μm). In B, the architecture is more disorganized (although this appearance may be enhanced by somewhat cross sectional orientation in this image), with separation of axonal fibers and increased glial cell profiles. Panels C (animal 1) and D (animal 3) present transmission electron microscopic images (bar = 5 μm) magnification each with insets at 30,000x (bar = 1 μm). The insets highlight axons (Ax) to illustrate dilated axons in animal 3 (D) compared to animal 1 (C). Mitochondria are indicated (m). Animal 2 had similar TEM findings as animal 3 (images not shown).

Table 1

Neonatal measurements collected during resuscitation of 4 primates delivered after *in utero* UCO to induce HIE. Blood gas and APGAR scores are all indicative of perinatal hypoxia-ischemia.

										APGAR Scores			
Animal	**Birth Weight (g)**	**Sex**	**Days Early**	**pH**	**BE**	**pCO_2**	**pO_2**	**HCO_3**	**Lactate**	**1**	**5**	**10**	**20**
1	561	M	−10	6.9	−20	67.9	94	13	14.8	1	2	2	5
2	459	M	−11	7.1	−19	36.3	279	10.9	13.2	1	3	3	3
3	526	F	−7	7.1	−19	29.8	87	10.1	12.7	1	2	4	4
4	461	F	−7	6.9	−25	40.1	232	7.7	17.8	1	3	4	4

UCO: umbilical cord occlusion, HIE: hypoxic ischemic encephalopathy, BE: base excess

Table 2

MRS concentrations at 8 days of age in animals who underwent umbilical cord occlusion for 18 minutes plus episodes of postnatal hypoxia (UCO + PH) exposure compared to an age-matched control animal and historical UCO and control animals.

Animal	Cho	Cr	NAA	Macm	Ins	Glu1	Glx	Cho/Cr	NAA/Cho	NAA/Cr
1	1.36	5.91	4.09	13.02	5.83	2.99	5.93	0.23	3.01	0.69
2	1.70	5.98	4.09	13.41	5.32	2.52	7.37	0.28	2.41	0.68
3	1.48	6.5	3.74	12.87	5.62	2.74	8.99	0.23	2.53	0.58
4	1.35	5.58	3.58	16.74	5.43	2.75	7.88	0.24	2.65	0.64
Control	1.55	4.82	4.23	7.89	4.19	3.20	8.87	0.32	2.72	0.88
UCO+PH	1.47±0.08		2.65±0.13					0.25±0.01	2.65±0.13	†0.65±0.03
*UCO_{18min}	1.63±0.07		4.03±0.10					0.30±0.01	2.50±0.13	0.73±0.02
*Control	1.60±0.05		4.3±0.09					0.29±0.01	2.79±0.08	0.79±0.02

*Comparison MRS data (bottom 3 rows) obtained at 24–72 hrs of age from historical control animals (n=12) and animals who underwent UCO for 18 min (n=13) without postnatal hypoxia (PH) exposure (from reference #8). Data for UCO+PH (n=4),

*UCO, and *Control are mean (±SEM) values.

†p=0.008 based on one-way ANOVA post hoc testing UCO+PH compared to UCO and controls.

Table 3

Mean (± SEM) mass spectral intensity values for metabolites in plasma from neonatal primates (N=4) before (0) and after UCO-induced HIE. Metabolites were detected by GC/GC/TOFMS, PARAFAC signal ratios selected the top 15 candidates, then repeated measures ANOVA and *post hoc* Dunnett's testing were performed. Section A lists metabolites that peaked immediately but declined (acute HIE response), section B lists those that increased gradually after birth (developmental response) and section C lists those that were not statistically different from baseline.

	Postnatal Age (h)		
	0	**0.1**	**24**
A)			
Arachidonic Acid	5 ± 1	18 ± 3**	10 ± 2
Fumaric Acid	3 ± 0	15 ± 2†	7 ± 1
Succinic Acid	11 ± 5	435 ± 58†	19 ± 2
Propanoic Acid	2611 ± 396	4089 ± 202*	1859 ± 244
B)			
Myoinositol	444 ± 54	834 ± 63*	1185 ± 121†
L-Glutamate	84 ± 11	203 ± 10	152 ± 18*
Choline	21 ± 5	15 ± 2	54 ± 11†
Glycine	74 ± 8	113 ± 20	230 ± 50*
L-Serine	147 ± 39	266 ± 44	447 ± 89*
Oleic Acid	125 ± 27	62 ± 6	322 ± 62*
Erythro-Pentonic Acid	3 ± 0	5 ± 1	19 ± 3†
C)			
Alanine	373 ± 48	519 ± 86	453 ± 70
Butanoic Acid	88 ± 23	129 ± 26	58 ± 19
Dextrose	2572 ± 316	4420 ± 238	3737 ± 587
Leucine	136 ± 33	251 ± 40	166 ± 27

Dunnett's test *vs.* 0h, *,**,† = P ≤ .05, .01, .001 respectively.

Table 4

Brain histopathology findings of four nonhuman primates exposed to *in utero* UCO to induce HIE and postnatal hypoxia episodes with necropsy on day of age 8

Animal	Thalamus and Striatum	Cerebral White Matter	Cerebral Gray Matter	Hippocampus	Cerebellum*	Brainstem
1	Acute neuronal necrosis and gliosis in ventrolateral thalamus; putamen/globus pallidus not affected	NDA	NDA	NDA	NDA	Diffuse gliosis, but no obvious apparent neuronal loss
2	Neuronal injury/loss and severe gliosis in small portion of ventrolateral thalamus; putamen/ globus pallidus not affected	Mild deep white matter gliosis	NDA	NDA	NDA	Large foci of neuronal injury/loss and severe gliosis in tegmentum of midbrain and pons and lateral medulla
3	Neuronal injury/loss and severe gliosis in large portion of ventrolateral thalamus and putamen/ globus pallidus	Mild deep white matter gliosis	NDA	NDA	NE	Large foci of neuronal injury/loss and severe gliosis in tegmentum of midbrain and pons and lateral medulla
4	Neuronal injury/loss and severe gliosis in large portion of ventrolateral thalamus and putamen/ globus pallidus	Mild deep white matter gliosis	NDA	NDA	Purkinje cell loss with Bergman gliosis	Large foci of neuronal injury/loss and severe gliosis in tegmentum of midbrain and pons and lateral medulla

NDA, no diagnostic alterations; NE, not evaluated;

*only small portion of cerebellum was sampled

UCO: umbilical cord occlusion, HIE: hypoxic ischemic encephalopathy